

See discussions, stats, and author profiles for this publication at: <https://www.researchgate.net/publication/270651132>

Whispering Gallery Mode Lasing from Hexagonal Shaped Layered Lead Iodide Crystals

ARTICLE *in* ACS NANO · JANUARY 2015

Impact Factor: 12.88 · DOI: 10.1021/nn5061207 · Source: PubMed

CITATIONS

6

READS

66

8 AUTHORS, INCLUDING:



Tung Son Ha

Nanyang Technological University

13 PUBLICATIONS 109 CITATIONS

[SEE PROFILE](#)



Jordi Arbiol

Catalan Institute of Nanoscience and Nanot...

347 PUBLICATIONS 7,603 CITATIONS

[SEE PROFILE](#)



Tze Chien Sum

Nanyang Technological University

143 PUBLICATIONS 3,509 CITATIONS

[SEE PROFILE](#)



Qihua Xiong

Nanyang Technological University

166 PUBLICATIONS 3,982 CITATIONS

[SEE PROFILE](#)

Whispering Gallery Mode Lasing from Hexagonal Shaped Layered Lead Iodide Crystals

Xinfeng Liu,^{†,‡,△} Son Tung Ha,^{†,△} Qing Zhang,[†] Maria de la Mata,[§] César Magen,[§] Jordi Arbiol,^{§,¶} Tze Chien Sum,^{*,†,‡,||} and Qihua Xiong^{*,†,‡,¶}

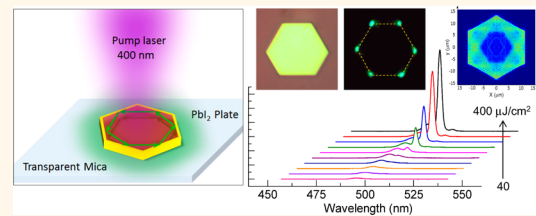
[†]Division of Physics and Applied Physics, School of Physical and Mathematical Sciences, Nanyang Technological University, Singapore 637371, Singapore,

[‡]Energy Research Institute @ NTU (ERI@N), Nanyang Technological University, 50 Nanyang Drive, Singapore 637553, Singapore, [§]Institut de Ciència de Materials de Barcelona, ICMAB-CSIC, E-08193 Bellaterra, CAT, Spain, [¶]Laboratorio de Microscopías Avanzadas (LMA), Instituto de Nanociencia de Aragón (INA)—ARAID and Departamento de Física de la Materia Condensada, Universidad de Zaragoza, 50018 Zaragoza, Spain, ^{*}Institució Catalana de Recerca i Estudis Avançats (ICREA), 08010 Barcelona, CAT, Spain, ^{||}Singapore-Berkeley Research Initiative for Sustainable Energy, 1 Create Way, Singapore 138602, Singapore, and

[#]NOVITAS, Nanoelectronics Centre of Excellence, School of Electrical and Electronic Engineering, Nanyang Technological University, Singapore 639798, Singapore.

△These authors contribute equally to this work.

ABSTRACT We report on the synthesis and optical gain properties of regularly shaped lead iodide (PbI_2) platelets with thickness ranging from 10–500 nm synthesized by chemical vapor deposition methods. The as-prepared single crystalline platelets exhibit a near band edge emission of ~ 500 nm. Whispering gallery mode (WGM) lasing from individual hexagonal shaped PbI_2 platelets is demonstrated in the temperature-range of 77–210 K, where the lasing modes are supported by platelets as thin as 45 nm. The finite-difference time-domain simulation and the edge-length dependent threshold confirm the planar WGM lasing mechanism in such hexagonal shaped PbI_2 platelet. Through a comprehensive study of power-dependent photoluminescence (PL) and time-resolved PL spectroscopy, we ascribe the WGM lasing to be biexcitonic in nature. Moreover, for different thicknesses of platelet, the lowest lasing threshold occurs in platelets of ~ 120 nm, which attributes to the formation of a good Fabry–Pérot resonance cavity in the vertical direction between the top and bottom platelet surfaces that enhances the reflection. Our present study demonstrates the feasibility of planar light sources based on layered semiconductor materials and that their thickness-dependent threshold characteristic is beneficial for the optimization of layered material based optoelectronic devices.



KEYWORDS: whispering gallery mode (WGM) · lasing · layered materials · lead iodide · hexagonal platelet · Fabry–Pérot cavity

Lead iodide (PbI_2), which consists of a repeating unit of a hexagonally closed-packed layer of lead ions sandwiched between two layers of iodide ions (layered material), has some unique optical and electronic properties that are quite different from traditional semiconductor gain material such as CdS, ZnO, and GaN.^{1–5} In these layered semiconductor materials (PbI_2 , BiI_3 , HgI_2 , Bi_2S_3 , and Sb_2S_3), spatial confinement of charge carriers in multi-layered or multiquantum-well structures has many potential utilities in photovoltaic, detectors, sensors, and photo catalysis.^{1,6,7} Additionally, this kind of layered material would provide us an ideal system to investigate the fundamental properties of excitons in a highly ionic environment and low dimensionality, where the exciton–phonon

coupling is expected to be unprecedented compared with conventional semiconductors.^{3,4}

On the other hand, PbI_2 has been extensively employed as a stable nuclear radiation detector.^{8–10} It converts the X-ray or γ -ray photons directly to electric charges (current carriers) that are stored in a capacitor in each pixel that improves the quality of the image compared with the traditional phosphorus layer. By working as a scintillation detector, many electron–hole pairs are first generated and thermalized in the conduction and valence bands after the absorption of the X-ray or γ -ray. Then, electrons and holes migrate through the material, trapping at defects may occur, and energy losses are probable because of nonradiative recombination. Therefore,

* Address correspondence to
Qihua@ntu.edu.sg,
Tzechien@ntu.edu.sg.

Received for review October 27, 2014
and accepted January 6, 2015.

Published online January 06, 2015
10.1021/nn5061207

© 2015 American Chemical Society

understanding the behavior of electron and hole under strong light excitation is beneficial to the design of the photodetector under relatively strong X- or γ -ray exposure intensities.

Moreover, PbI_2 is one of the precursors to synthesize lead halide perovskites, which have shown tremendous advances in photovoltaics for the past few years and have also been demonstrated as a promising optical gain material for amplified spontaneous emission (ASE) or lasing.^{11–13} Deep investigations of the lead halides precursor (*e.g.*, lead iodide) are important toward the understanding of the photophysics of the inorganic–organic perovskites and their applications in emergent devices.^{14,15} From previous literature, the optical and excitonic properties of single crystalline PbI_2 films and thin layers have been previously investigated by steady-state and ultrafast spectroscopy techniques.^{7,16–20} As for their synthesis, several special experimental methods have been developed involving the sol–gel method,²⁰ vapor deposition method,²¹ and Bridgman's method for growth of PbI_2 single crystals.^{5,22} However, challenges pertaining to the synthesis of regular-shaped single crystalline PbI_2 crystals with subwavelength thickness, ideal for on-chip optical amplifier and lasers integration with planar optoelectronic devices, remain daunting. Despite the limited work on linear optical properties, the studies that focus on the recombination and amplification of photon emission in layered PbI_2 platelets under strong optical excitation are still limited.^{23,24}

In this work, we have synthesized regular-shaped PbI_2 platelet with thickness ranging from 10–500 nm using a chemical vapor deposition (CVD) method. The as-prepared single crystalline platelets exhibit a near band gap emission of \sim 500 nm at 77 K. Whispering gallery mode (WGM) lasing from PbI_2 is demonstrated from individual platelets at temperatures from 77–210 K. Lasing modes are supported in PbI_2 platelets as thin as 45 nm, which is the thinnest planar laser ever reported. Through a comprehensive power-dependent photoluminescence (PL) and time-resolved photoluminescence (TRPL) study, we establish unambiguously that the lasing mechanism originates from biexcitonic recombination. Thickness-dependent lasing measurements reveal that the lowest lasing threshold occurs when the platelet thickness is \sim 120 nm. We attribute this thickness-dependent behavior of the lasing threshold to the reflection between the top and bottom surfaces of PbI_2 that form the Fabry–Pérot (F–P) resonance cavity in the vertical direction. Our experiment results demonstrate the feasibility of planar light sources based on layered semiconductor materials.

RESULTS AND DISCUSSION

The synthesis procedure of PbI_2 single crystals can be found in the Methods section. The as-grown PbI_2

platelets exhibit well-defined triangular or hexagonal structures with thickness ranging from 10–500 nm and the edge lengths from several to tens of micrometers (hexagonal shaped PbI_2 platelet was our main focus in this work). Figure 1, panels a–d exhibit the optical images of four typical shaped as-grown PbI_2 platelets. Their thicknesses are around 40, 70, 105, and 500 nm, respectively, which is determined by the atomic force microscopy (AFM) data (Supporting Information, Figure S1). The average surface roughness of these PbI_2 platelets is \sim 2 nm, which is perfectly flat at optical level. The flat surface is an essential criterion to achieve a high quality optical cavity. The X-ray diffraction pattern shown in Figure S2 suggests the 2H hexagonal crystalline structure. Raman spectroscopy characterization of the as-prepared sample in Figure S3 also suggests the forming of PbI_2 crystals. More detailed characterization was also carried out using transmission electron microscopy (TEM) and a scanning TEM (STEM) to assess the structure, crystallinity, and elemental composition of the as-grown PbI_2 sample. Figure 1, panel e is a typical TEM image of the PbI_2 platelet; Figure 1, panels f and g give the corresponding Pb and I mapping images obtained by energy dispersive X-ray spectroscopy, which confirms the elemental uniformity of the as-grown PbI_2 platelet over the whole platelet. The high-resolution cross-sectional TEM image (see Figure 1h) of the platelet shows that the interlayer space is around 0.703 nm, which is in good agreement with the (0001) plane spacing theoretical value.^{25,26} The atomic structures of the layer atoms in planar view are also studied by high-resolution TEM (HRTEM). Figure 1, panel i is the HRTEM image of the layer PbI_2 , where the middle inset overlapping the structure corresponds to the simulated HRTEM image. Notice that red and blue dashed circles represent the positions of top/lower-layer of iodine atoms, which are indistinguishable from the HRTEM images according to the image simulations performed. In the center position encircled by these iodine atoms is the Pb atom, which is relatively brighter compared to the iodine atoms, which is also in good agreement with our HRTEM image simulations. Figure 1, panel i, bottom inset shows the corresponding fast Fourier transform (FFT) pattern of the HRTEM image showing the six-fold symmetric diffraction spot, which is consistent with our XRD results. All these characterizations attest the high crystallinity of these as-synthesized PbI_2 platelets, which is an important factor for achieving photon amplification in these naturally formed whispering gallery cavities.

An individual PbI_2 platelet was optically pumped using 400 nm wavelength femtosecond laser pulses at 77 K. The optical pump configuration is schematically shown in Figure 2, panel a. The pump laser was focused to a spot size of \sim 40 μm using a 20 \times objective. Figure 2, panel b shows the power-dependent

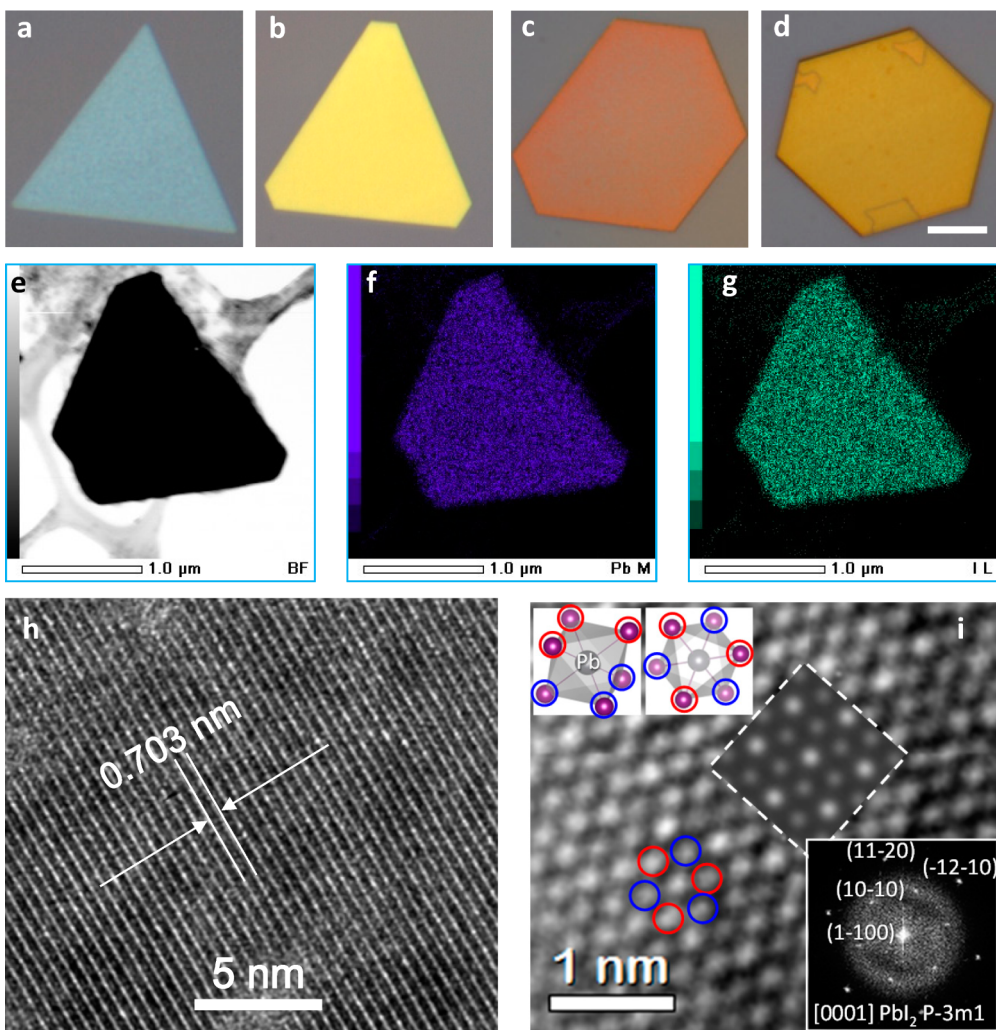


Figure 1. Chemical-vapor-deposited PbI_2 platelets and characterization. (a–d) Optical images of four representative PbI_2 platelets with different thicknesses of 40, 70, 105, and 500 nm. These platelets show planar, well-defined, polygonal structures. The angles between the polygonal edges are 30° , 60° , or 120° , which is consistent with the atomic structures of PbI_2 . The scale bar is $5\ \mu\text{m}$. (e) TEM image of a PbI_2 platelet. (f, g) The element mapping images obtained by energy-dispersive X-ray spectroscopy show the uniformity of the platelet of PbI_2 . (h) HRTEM structural analysis of the cross-section of single-crystalline PbI_2 platelet, which shows a layer spacing of around $0.703\ \text{nm}$. (i) High resolution TEM (HRTEM) image showing the hexagonal structure of the PbI_2 ; red dash circle (bright spot) is the top-layer iodine atom, blue dash circle (dim spot) is the lower-layer iodine atom, the center position is the Pb atom. Top inset is a sketch of the PbI_2 structure from the top view; bottom inset is the fast Fourier transform pattern from the HRTEM image.

emission spectra of a typical PbI_2 hexagonal platelet (thickness $\sim 150\ \text{nm}$; edge length $\sim 13\ \mu\text{m}$). A broad spontaneous emission band centered at $500\ \text{nm}$ with a full width at half-maximum (fwhm) of $\lambda_{\text{fwhm}} \approx 6\ \text{nm}$ can be observed under relatively lower pump fluence excitation (e.g., $P < 100\ \mu\text{J}/\text{cm}^2$). With increased pump fluence ($\sim 200\ \mu\text{J}/\text{cm}^2$), a relatively sharp peak centered at around $502\ \text{nm}$ with a λ_{fwhm} of $\sim 3.5\ \text{nm}$ appears at the longer wavelength side of the main spontaneous emission peak. When the pump fluence is further increased ($P > 200\ \mu\text{J}/\text{cm}^2$), the emission peak intensity increases sharply, and the fwhm of the emission peak reduces to $\sim 1.4\ \text{nm}$, which exhibits lasing action.^{27,28} The inset of Figure 2, panel b shows the peak emission intensity as a function of excitation intensity (light input–light output, or “ L – L curve”, right axis) and

the fwhm of the platelet emission (left axis). At the lasing threshold $P_{\text{th}} \sim 200\ \mu\text{J}/\text{cm}^2$, we observed a clear change in gradient in the L – L curve with a concurrent sharp decrease in fwhm. Beyond the threshold, the lasing peak intensity increases linearly with excitation fluence. It should be noted that only one peak is observed in the micrometer cavity, which probably results from the broadening of lasing modes due to the fact that these lasing modes share almost the same threshold at low temperature range. TRPL study is employed (see Figure 2c,d) to further validate the occurrence of the lasing action. Below the threshold, an Auger-limited spontaneous emission lifetime of $\sim 70\ \text{ps}$ is obtained. Above the threshold, the PL dynamics at the emission peak show a dominant ultrafast decay channel with a lifetime of $\sim 10\ \text{ps}$

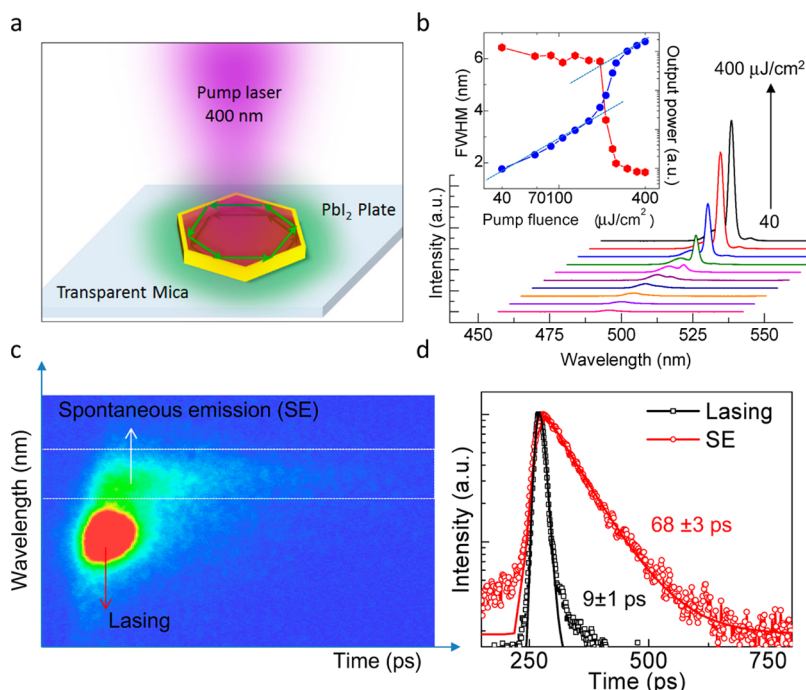


Figure 2. Lasing characterizations of whispering gallery mode hexagonal PbI_2 platelet. (a) Schematic representation of a single PbI_2 platelet excited by a focused femtosecond pulse laser. (b) The evolution from spontaneous emission to lasing in a typical PbI_2 hexagonal platelet; the pumping fluence increased from 40 to $400 \mu\text{J}/\text{cm}^2$. The inset shows power dependence of the integrated intensity and line width of the dominant emission feature, which gives a threshold of $\sim 200 \mu\text{J}/\text{cm}^2$. (c) A streak camera image of PbI_2 platelet emission when the excitation fluence is above the threshold. (d) The decay profiles of the SE and lasing action are fitted using a monoexponential decay function yielding lifetimes of 68 ± 3 and 9 ± 1 ps for SE and lasing, respectively.

(limited by the system response of the streak camera over the time window) and a small spontaneous emission component with a lifetime of ~ 70 ps.

To prove that WGM lasing occurs in the hexagonal shaped PbI_2 platelet, optical mode simulations are performed to study the field distribution in the resonant cavity modes. Optical simulations are performed using commercial finite-difference time-domain (FDTD) simulation software (Lumerical) to study the mode distribution in PbI_2 platelet grown on mica substrate. To simplify the system from 3D to 2D, we introduce the effective index of refraction, mainly the planar waveguide model. Then we simulate the mode distribution in 2D system using the effective index rather than the index of the material. Figure 3, panel a shows an optical image of a representative hexagonal PbI_2 platelet with thickness ~ 150 nm and edge length $\sim 13 \mu\text{m}$, respectively. The PL emission image (the excitation laser was filtered out by a long pass filter) of the same hexagonal PbI_2 platelet above the lasing threshold can be clearly seen in Figure 3, panel b. The bright spots at the hexagonal corners indicate the out coupling of the laser pulses at these locations. It suggests that a good mode confinement in the platelet plane is obtained, leading to an in-plane emission. Figure 3, panels c and d show the simulation results on the absolute electric field distribution inside the hexagonal platelet (thickness ~ 150 nm; edge length $\sim 13 \mu\text{m}$) when the transverse magnetic (TM, effective index ~ 2.18) and transverse electric

(TE, effective index ~ 1.97) modes dominate, respectively. In these two scenarios, the optical fields are well confined inside the cavities, and reflections between the hexagonal facets/corners result in the formation of the WGMs. However, compared to the TE mode, the TM mode has a larger effective refractive index (the TM and TE modes should not be the same order because the effective index is generally higher for TE than TM mode of the same order) and relatively strong field intensity; thus, a lower lasing threshold can be expected from the TM mode.²⁹ This is evident from the similarity between the optical image (see Figure 3b) and TM mode simulations (see Figure 3c). To experimentally prove our simulation result, using confocal microscopy system, we measured the polarization-dependent lasing intensities. The measured polarization-dependent lasing intensity is exhibited in Figure S4. It can be seen that the lasing intensity shows a maximum when the polarization is along the 0 degree axis, which suggests that the TM mode dominates the signal (if the TE mode dominates, the maximum signal happens when the polarization angle is in 90 degree direction). Another evidence to confirm the WGM mode lasing rather than F-P lasing in the vertical direction is the $1/L^2$ relationship between the platelet edge length (L) and the lasing threshold. The related data and discussion will be shown in the later part.

To elucidate the lasing mechanism, pump fluence dependent time-integrated PL of a single PbI_2

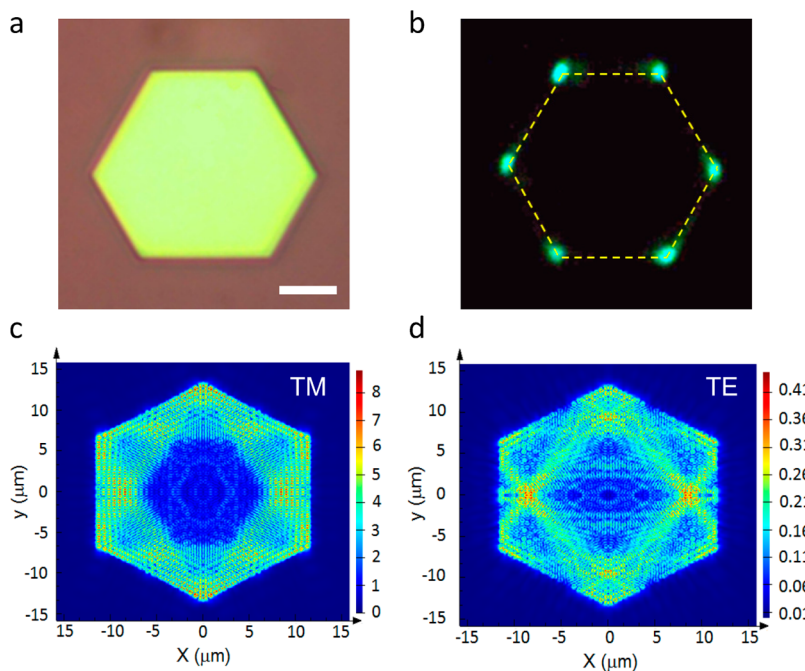


Figure 3. FDTD simulation of the electric distribution inside the cavity for hexagonal PbI₂ platelet. (a) The optical image of a hexagonal platelet with thickness of ~ 150 nm and edge length ~ 13 μm . The scale bar is 5 μm . (b) The optical image in the charge-coupled device (CCD) after filtering of the pump laser line for a pump fluence of ~ 350 $\mu\text{J}/\text{cm}^2$ (above threshold). (c, d) Simulated field distribution at resonant cavity mode of the typical hexagonal PbI₂ platelets using (c) TM and (d) TE mode.

platelet at 77 K is performed, and the results are given in Figure 4, panel a. The inset shows a representative PL spectrum (with a pumping fluence ~ 40 $\mu\text{J}/\text{cm}^2$) with two dominant peaks labeled as Peak X and Peak XX, which are deconvolved from the Gaussian fitting of the broad emission peak. The intensity of Peak X (centered at 498 nm) is linearly proportional (slope ~ 0.95) to the excitation fluence when it is below ~ 90 $\mu\text{J}/\text{cm}^2$ and then increases as the square-root of the excitation fluence above that. On the other hand, Peak XX (centered at 505 nm) exhibits a quadratic dependence with excitation fluence up to ~ 20 $\mu\text{J}/\text{cm}^2$ and then increases almost linearly proportional (with slope ~ 0.9) to the excitation fluence up to ~ 200 $\mu\text{J}/\text{cm}^2$. Beyond that, Peak XX increases superlinearly with pump fluence to yield a lasing action. Such pump fluence dependent emission characteristics of Peaks X and XX closely resemble those of exciton and biexciton luminescence reported for Si, GaN/AlN, and perovskite materials, respectively.^{30–32} Therefore, we attribute the emissions at Peaks X and XX to originate from the single exciton and biexciton emission, respectively.³³ Radiative recombination of a biexciton produces a photon ($\hbar\omega_{XX}$) and an exciton (E_X), and hence, $\hbar\omega_{XX} = E_{XX} - E_X = E_X + \Delta_{XX}$, where E_{XX} is biexciton recombination energy, and Δ_{XX} is the biexciton binding energy.^{34,35} The biexciton binding energy, ~ 32 meV, can be deduced from the energy difference between the single exciton E_X ($\hbar\omega_X$) and biexciton $\hbar\omega_{XX}$, which agrees with the value of ~ 30 meV reported previously.³⁶ The PL decay transients of the

single excitons (Peak X) and the biexcitons (Peak XX) both exhibit a monoexponential decay behavior (see Figure 4b) and can be well-fitted with a single recombination lifetime of $\sim 83 \pm 4$ ps and 47 ± 3 ps for the excitons and biexcitons, respectively.^{37,38} The ratio of biexciton lifetime versus that of the exciton is ~ 1.8 ; which is very close to the intuitive relation of $\tau_X/\tau_{XX} = 2$, where a biexciton is treated like a system of two weakly coupled excitons with half the exciton's lifetime.^{39,40}

After the lasing mechanism was validated to be biexcitonic in origin, we turned our attention to the intrinsic lasing properties (*i.e.*, wavelength and threshold) as a function of temperature. Figure 4, panel c shows the normalized emission spectra recorded at the above threshold for a single PbI₂ platelet from 77–210 K, with the pumping fluence of 0.25, 0.4, 0.7, 1.2, and 2.5 mJ/cm², respectively. When the temperature increases to be higher than 210 K, the lasing action ceases for the PbI₂ platelet. As the lattice temperature varies, the dominant lasing peak redshifts (see Figure 4d) from 496 to 510 nm, which suggests a bandgap narrowing.^{41,42} Furthermore, the lasing peak is always located at the longer wavelength side of the broad emission peak. It means that the lasing behavior is always related to the biexciton formation and recombination at this temperature range (77–210 K). The lasing threshold increases from ~ 200 $\mu\text{J}/\text{cm}^2$ to ~ 2.3 mJ/cm² when the sample temperature increases from 77 to 210 K (see Figure 4d). This behavior can be fitted by an exponential function (lasing threshold $\sim e^{T/T_0}$) that describes the thermal broadening of

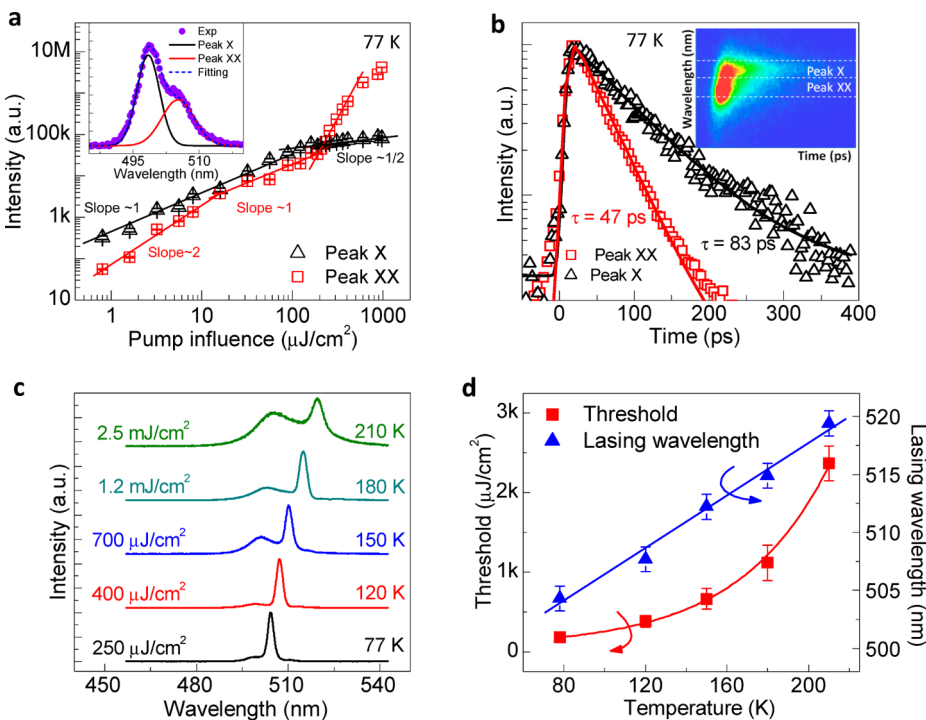


Figure 4. Lasing mechanism and intrinsic properties of PbI_2 platelet. (a) Excitation power dependent emission intensities of Peak X (open triangles) and Peak XX (open squares) in PbI_2 platelet at 77 K. Inset is the Gaussian fitting of PL spectra (at excitation fluence of $\sim 40 \mu\text{J}/\text{cm}^2$) of PbI_2 ; the black fitting curve is band X, and the red fitting line is band XX. (b) TRPL spectra of Peaks X and XX, and the inset is the corresponding time-energy two-dimensional image of the PL emission. The pump fluence is fixed at $\sim 40 \mu\text{J}/\text{cm}^2$ at 77 K. The decay profiles of Peaks X and XX are fitted with a mono-exponential function, and the lifetimes are 83 ± 3 ps and 47 ± 2 ps, respectively. (c) The lasing spectra of a PbI_2 platelet at different temperatures (from 77–210 K). (d) Temperature-dependent lasing threshold and lasing wavelength of PbI_2 are summarized. The blue line is the linear fitting, and the red curve is the exponential function fitting result.

the gain spectrum, and we obtain a characteristic temperature of $T_0 = 45$ K for the PbI_2 platelet laser (see Figure 4d). This characteristic temperature is the description of the thermal stability of this material, which explains why no lasing can be obtained at room temperature. On the contrary, some conventional semiconductors exhibit higher characteristic temperatures, for example, 90–130 K for ZnO and 160–246 K for GaN.^{43,44}

Since the different platelet size (i.e., edge length L) affects the mode confinement and hence the lasing threshold,⁴⁵ we carefully conducted this study using a series of hexagonal PbI_2 platelets with similar edge lengths (i.e., $20 \pm 2 \mu\text{m}$) while we investigated the thickness-dependent lasing properties. Figure 5, panels a–d show the PL spectra from four typical PbI_2 platelets with different thicknesses when they are optically pumped by a pulsed laser at 77 K. The thicknesses of PbI_2 in Figure 5, panels a–d are 40, 120, 200, and 300 nm, respectively. At lower pump fluence, the PL spectra are broad; however, as the pump influence increased above the lasing threshold, a sharp peak at around 500 nm occurs with a fwhm of 1 nm. A plot of the intensity peak versus pump fluence (insets of Figure 5a–d) shows the transition from spontaneous to stimulated emission. The corresponding thresholds for the 40, 120, and 300 nm thick PbI_2

platelets are 442, 54, and 280 $\mu\text{J}/\text{cm}^2$, respectively. Figure 5, panel e summarizes the PbI_2 lasing threshold with different thickness ranging from 45–300 nm. It is very interesting that the lowest lasing threshold occurs when the layer thickness is ~ 122 nm. In addition, another local minimum is observed at ~ 245 nm.

To investigate the layer thickness dependence of the lasing threshold, the parametric threshold gain, G_{th} , is used here to describe our current system. The expression of G_{th} is defined as follows, $G_{\text{th}} = 2\pi n_g / (\Gamma_E \lambda Q)$, where n_g , λ , Γ_E , and Q are group index of the material, resonant wavelength, energy confinement factor, and quality factor, respectively.⁴⁶ Since this expression originates from the general gain and loss balance conditions for the rate equation, it is valid for all types of cavity modes. In the case of PbI_2 platelets, the group index and resonant wavelength can be treated approximately independent of the platelet thickness. Furthermore, the lasing modes of PbI_2 for different thicknesses have almost the same peak width (~ 1 nm), which indicates comparable Q factors. Therefore, the energy confinement factor Γ_E should play as the dominant role in our scenario. Because of the large edge length ($\sim 20 \mu\text{m}$) of PbI_2 , the WGM loss in the planar direction can be negligible compared to the loss in the vertical direction owing to subwavelength thickness ranging from 40–300 nm. However, in the vertical

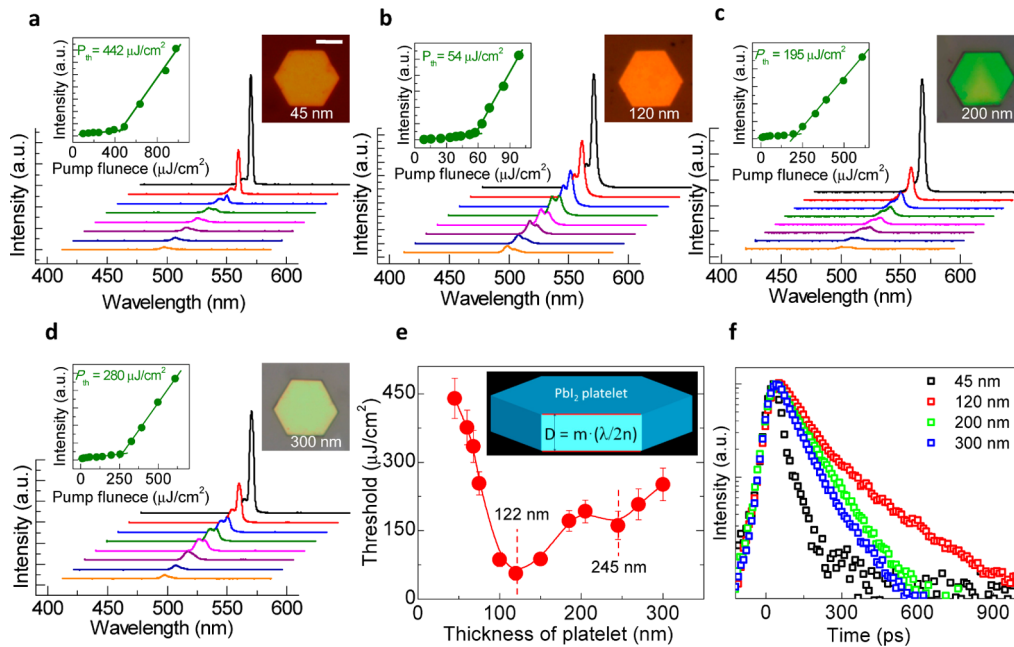


Figure 5. Thickness-dependent lasing thresholds in hexagonal PbI_2 platelets. (a–d) PbI_2 hexagonal platelets emission spectra with increasing pump fluence from below threshold to above threshold; inset left is the plot of wavelength *versus* emission intensity, which shows the threshold of the sample; inset right is the optical image of the hexagonal platelet. The thicknesses of the platelet in panels a, b, c, and d are ~ 45 , 120 , 200 , and 300 nm, respectively. To reduce the influence of edge length of hexagonal platelet to the threshold of lasing, hexagonal platelets with nearly the same edge length are carefully selected for the study. The scale bar is $10 \mu\text{m}$. (e) Thickness-dependent lasing threshold in a triangular PbI_2 platelet; two dips or minima located at 122 and 245 nm are observed for low pump thresholds. (f) Decay profile of the biexciton peak (Peak XX) of the PbI_2 hexagonal platelet with different thickness when excited at the same pump fluence of $\sim 60 \mu\text{J}/\text{cm}^2$.

direction, the top and bottom surfaces of the PbI_2 platelet function as mirrors by forming a F–P cavity itself. This naturally formed F–P cavity holds maximum energy confinement when the cavity length (D) satisfies the following equation, $D \times n_{\text{PbI}_2} = m \times \lambda/2$ (see the inset of Figure 5e), where λ and n_{PbI_2} are resonant wavelength and refractive index, respectively, while m is an integer.^{47,48} Considering that the lasing wavelength is ~ 505 nm and refractive index of PbI_2 at 505 nm is ~ 2.1 , PbI_2 platelets with thicknesses of ~ 120 nm and ~ 240 nm would possess the maximum energy confinement (Γ_E) for thickness in the range from 45 – 300 nm range, which would then lead to the lowest threshold at these two thickness. This is in good agreement with our experimental observations of the two lowest threshold pump fluences at 122 and 245 nm (see Figure 5e). Furthermore, another proof is the biexciton lifetime measurement (with the same excitation power of $\sim 40 \mu\text{J}/\text{cm}^2$) for the PbI_2 platelets of varying thicknesses, as shown in Figure 5, panel f. It is interesting to note that the 120 nm thick PbI_2 platelet exhibits the longest biexciton lifetime. Intuitively, this agrees well with the occurrence of the lowest pump threshold as the longer lived biexciton population would facilitate the population inversion and the buildup of lasing in photonic mode lasing conditions. Moreover, the maximum PL intensity for the 120 nm thick PbI_2 platelet (see Figure S5) further supports our argument. Therefore, we can conclude that the lasing

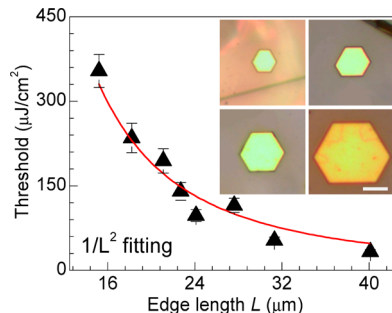


Figure 6. Lasing thresholds *versus* edge length of the hexagonal PbI_2 platelets. PbI_2 hexagonal platelets lasing thresholds (black triangles) are plotted as a function of edge length. The red curve is the fitting to a $1/L^2$ trend. Inset are the optical images of a group of PbI_2 triangular platelets with different edge lengths but comparable thickness of 200 ± 20 nm; the scale bar inside is $15 \mu\text{m}$.

behavior in hexagonal PbI_2 structure is predominately determined by the planar WGM modes and is also partially affected by the thickness of the platelet.

Lastly, a plot of hexagonal PbI_2 platelet edge length (L) versus lasing threshold is shown in Figure 6. To minimize the effect of different thicknesses, a series of PbI_2 platelets with comparable thickness (~ 200 nm) but different edge lengths (from 14 – $40 \mu\text{m}$) were selected for this study (see inset in Figure 6). The best-fit line (red curve) is approximately $1/L^2$, which indicates that the lasing threshold is dominantly dependent on the parameter of PbI_2 platelet edge

length. Previous studies have shown that both WGM quality factor (Q) and confinement factor (Γ) depend critically on disk diameter.^{46,49,50} Since lasing threshold is inversely proportional to Q and Γ , a $1/L^2$ relationship is expected for platelet edge length and lasing threshold. By considering the thickness-dependent threshold discussion, we know that the lasing threshold scales inversely with the power of platelet edge length, rather than with platelet thickness. This provides clear evidence of WGM lasing rather than F-P lasing in the vertical direction. This conclusion is consistent with our previous simulation results as shown in Figure 3, panel c.

CONCLUSIONS

In summary, we have demonstrated WGM lasing in single crystalline hexagonal PbI_2 platelet fabricated

using CVD method. Through power-dependent PL and TRPL studies, we establish that the lasing mechanism originates from biexciton recombination. Platelet thickness dependent lasing measurements reveal that the lowest threshold of lasing occurs when the thickness of the platelet is ~ 120 nm for a series of PbI_2 platelets with comparable edge length. This thickness-dependent behavior of threshold can be well explained by the reflection enhancement in the F-P resonance cavity in the vertical direction as validated by the lifetime measurements. Our results demonstrate the feasibility of planar coherent light sources based on layered semiconductor materials, and the thickness-dependent threshold study is of vital importance for the optimization of layered material based optoelectronic devices.

METHODS

PbI_2 Synthesis Process. Lead iodide powder (Aldrich, 99.999%) was the reaction source and placed into a quartz tube, which is amounted on a single zone furnace (Lindberg/Blue M TF55035C-1). Fresh cleaved muscovite mica substrate ($1 \times 3 \text{ cm}^2$) was cleaned by acetone and then placed in the downstream region inside the quartz tube. The quartz tube was evacuated to a base pressure of 2 mTorr and then followed by a 30 sccm flow of high-purity Ar premixed with 5% H_2 gas. The temperature and pressure inside the quartz tube were set and stabilized to desired values for each halide (380°C , 200 Torr). The synthesis process was finished within 20 min, and then the furnace cooled down to room temperature naturally.

Steady-State and Time-Resolved Photoluminescence Spectroscopy. The excitation pulses (wavelength, 400 nm) are double frequencies from the Coherent Libra regenerative amplifier (50 fs, 1 kHz, 800 nm), which is seeded by a Coherent Vitesse oscillator. The pump laser is focused onto samples by a $20\times$ objective. The laser spot is $\sim 40 \mu\text{m}$ in diameter after objective. For lasing images of the sample, the PL emission signals are imaged on a CCD camera using a long-pass filter to block the laser line. For spectrum measurement, the emission signals from an area ($\sim 5 \mu\text{m} \times 5 \mu\text{m}$) pass through an aperture and are analyzed by a spectrometer equipped with a TE-cooled CCD. For TRPL measurement, the PL emission was collected and dispersed by a 25 cm spectrometer using a 150 g/mm grating. The signal was resolved using an Optronics Streak Camera system (Optoscope), which has an ultimate temporal resolution of ~ 10 ps.

Numerical Simulation. Cavity simulations are performed using commercial FDTD simulation software (Lumerical) to study the optical feedback mechanism that allows laser oscillation in PbI_2 platelet grown on mica substrate.⁵¹ To simplify the system from 3D to 2D, we introduce the effective index of refraction, mainly the planar waveguide model. Then, we simulate the mode distribution in 2D system using the effective index rather than the index of the material. The refractive index of mica and PbI_2 can be obtained from the literature.^{16,17}

Conflict of Interest: The authors declare no competing financial interest.

Acknowledgment. Q.X. acknowledges the support from the Singapore National Research Foundation through a NRF fellowship grant (NRF-RF2009-06) and a Competitive Research Program grant (NRF-CRP-6-2010-2), the Ministry of Education AcRF Tier 2 grants (MOE2011-T2-2-051 and MOE2013-T2-1-049), and the start-up grant support (M58113004) from Nanyang Technological University (NTU). T.C.S. acknowledges the support from the following research grants: NTU start-up grant (M4080514); SPMS collaborative Research Award (M4080536);

and the Ministry of Education (MOE) Academic Research Fund (AcRF) Tier 2 Grant No. MOE2013-T2-1-081. X.F.L. and T.C.S. also acknowledge the financial support by the Singapore National Research Foundation through the Competitive Research Programme under Project No. NRF-CRP5-2009-04 and the Singapore-Berkeley Research Initiative for Sustainable Energy (SinBerRISE) CREATE Programme. J.A. acknowledges the funding from Generalitat de Catalunya 2014 SGR 1638. M.d.I.M. thanks the CSIC Jae-Predoc program.

Supporting Information Available: Optical images and the corresponding thicknesses of four representative PbI_2 platelets. XRD pattern of the as-prepared sample on mica. Raman spectra of the as-prepared platelets with different thicknesses. FDTD simulation results of the electrical distribution inside the cavity (TM mode). PL spectra of PbI_2 platelets with different thicknesses. This material is available free of charge via the Internet at <http://pubs.acs.org>.

REFERENCES AND NOTES

- Sengupta, A.; Jiang, B.; Mandal, K. C.; Zhang, J. Z. Ultrafast Electronic Relaxation Dynamics in PbI_2 Semiconductor Colloidal Nanoparticles: A Femtosecond Transient Absorption Study. *J. Phys. Chem. B* **1999**, *103*, 3128–3137.
- Makino, T.; Watanabe, M.; Hayashi, T.; Ashida, M. Time-Resolved Luminescence of Exciton Polaritons in PbI_2 . *Phys. Rev. B* **1998**, *57*, 3714–3717.
- Watanabe, M.; Hayashi, T. Polariton Relaxation and Bound Exciton Formation in PbI_2 Studied by Excitation Spectra. *J. Phys. Soc. Jpn.* **1994**, *63*, 785–794.
- Dorner, B.; Ghosh, R. E.; Harbeke, G. Phonon Dispersion in the Layered Compound PbI_2 . *Phys. Status Solidi B* **1976**, *73*, 655–659.
- Ahuja, R.; Arwin, H.; Ferreira da Silva, A.; Persson, C.; Osorio-Guillén, J. M.; Souza de Almeida, J.; Moyses Araujo, C.; Veje, E.; Veissid, N.; An, C. Y.; et al. Electronic and Optical Properties of Lead Iodide. *J. Appl. Phys.* **2002**, *92*, 7219–7224.
- Sandroff, C.; Hwang, D.; Chung, W. Carrier Confinement and Special Crystallite Dimensions in Layered Semiconductor Colloids. *Phys. Rev. B* **1986**, *33*, 5953–5955.
- Goto, T.; Tanaka, H. Exciton Study in PbI_2 Microcrystallites by Pump–Probe Method. *Solid State Commun.* **1994**, *89*, 17–21.
- Street, R. A.; Ready, S. E.; Van Schuylenbergh, K.; Ho, J.; Boyce, J. B.; Nylen, P.; Shah, K.; Melekhov, L.; Hermon, H. Comparison of PbI_2 and HgI_2 for Direct Detection Active Matrix X-ray Image Sensors. *J. Appl. Phys.* **2002**, *91*, 3345–3355.

9. Nikl, M. Scintillation Detectors for X-rays. *Meas. Sci. Technol.* **2006**, *17*, R37.
10. Yanagida, T.; Fujimoto, Y.; Yoshikawa, A.; Yokota, Y.; Kamada, K.; Pejchal, J.; Chani, V.; Kawaguchi, N.; Fukuda, K.; Uchiyama, K.; et al. Development and Performance Test of Picosecond Pulse X-ray Excited Streak Camera System for Scintillator Characterization. *Appl. Phys. Express* **2010**, *3*, 056202.
11. Zhang, Q.; Ha, S. T.; Liu, X.; Sum, T. C.; Xiong, Q. Room-Temperature Near-Infrared High-Q Perovskite Whispering Gallery Planar Nanolasers. *Nano Lett.* **2014**, *14*, 5995–6001.
12. Xing, G.; Mathews, N.; Lim, S. S.; Yantara, N.; Liu, X.; Sabba, D.; Grätzel, M.; Mhaisalkar, S.; Sum, T. C. Low-Temperature Solution-Processed Wavelength-Tunable Perovskites for Lasing. *Nat. Mater.* **2014**, *13*, 476–480.
13. Gratzel, M. The Light and Shade of Perovskite Solar Cells. *Nat. Mater.* **2014**, *13*, 838–842.
14. Tan, Z.-K.; Moghaddam, R. S.; Lai, M. L.; Docampo, P.; Higler, R.; Deschler, F.; Price, M.; Sadhanala, A.; Pazos, L. M.; Credgington, D.; et al. Bright Light-Emitting Diodes Based on Organometal Halide Perovskite. *Nat. Nanotechnol.* **2014**, *9*, 687–692.
15. Lin, Q.; Armin, A.; Nagiri, R. C. R.; Burn, P. L.; Meredith, P. Electro-Optics of Perovskite Solar Cells. *Nat. Photonics* [Online early access]. DOI: 10.1038/nphoton.2014.284. Published Online: December 1, **2014**.
16. Ahmad, A.; Saq'an, S.; Lahloub, B.; Hassan, M.; Alsaad, A.; El-Nasser, H. Ellipsometric Characterization of PbI_2 Thin Film on Glass. *Physica B* **2009**, *404*, 1–6.
17. Dugan, A. E.; Henisch, H. K. Dielectric Properties and Index of Refraction of Lead Iodide Single Crystals. *J. Phys. Chem. Solids* **1967**, *28*, 971–976.
18. Yamamoto, A.; Nakahara, H.; Yano, S.; Goto, T.; Kasuya, A. Exciton Dynamics in PbI_2 Ultra-Thin Microcrystallites. *Phys. Status Solidi B* **2001**, *224*, 301–305.
19. Ando, M.; Yazaki, M.; Katayama, I.; Ichida, H.; Wakaiki, S.; Kanematsu, Y.; Takeda, J. Photoluminescence Dynamics Due to Biexcitons and Exciton–Exciton Scattering in The Layered-Type Semiconductor PbI_2 . *Phys. Rev. B* **2012**, *86*.
20. Lifshitz, E.; Yassen, M.; Bykov, L.; Dag, I.; Chaim, R. Photo-decomposition and Regeneration of PbI_2 Nanometer-Sized Particles, Embedded in Porous Silica Films. *J. Phys. Chem.* **1995**, *99*, 1245–1250.
21. Fornaro, L.; Saucedo, E.; Mussio, L.; Gancharov, A. Toward Epitaxial Lead Iodide Films for X-ray Digital Imaging. *IEEE Trans. Nucl. Sci.* **2002**, *49*, 2274–2278.
22. Ferreira da Silva, A.; Veissid, N.; An, C. Y.; Pepe, I.; Barros de Oliveira, N.; Batista da Silva, A. V. Optical Determination of the Direct Bandgap Energy of Lead Iodide Crystals. *Appl. Phys. Lett.* **1996**, *69*, 1930–1932.
23. Brodin, M. S.; Vitrikovskii, N. I.; Kipen', A. A.; Yamkovaya, L. N.; Yanushevskii, N. I. Influence of Crystal Size and Temperature on the Stimulated Emission Spectrum of CuBr . *Quantum Electron.* **1989**, *19*, 324.
24. Brodin, M. S.; Blonskii, I. V.; Dobrovolskii, A. A.; Karataev, V. N.; Kipen', A. A.; Yanushevskii, N. I. Lasing in Laminar PbI_2 Single Crystals. *Quantum Electron.* **1986**, *16*, 140.
25. Sandroff, C. J.; Kelty, S. P.; Hwang, D. M. Clusters in Solution-Growth and Optical Properties of Layered Semiconductors with Hexagonal and Honeycombed Structures. *J. Chem. Phys.* **1986**, *85*, 5337–5340.
26. Zheng, Z.; Liu, A. R.; Wang, S. M.; Wang, Y.; Li, Z. S.; Lau, W. M.; Zhang, L. Z. In Situ Growth of Epitaxial Lead Iodide Films Composed of Hexagonal Single Crystals. *J. Mater. Chem.* **2005**, *15*, 4555–4559.
27. Saxena, D.; Mokkapati, S.; Parkinson, P.; Jiang, N.; Gao, Q.; Tan, H. H.; Jagadish, C. Optically Pumped Room-Temperature GaAs Nanowire Lasers. *Nat. Photonics* **2013**, *7*, 963–968.
28. Liu, X.; Zhang, Q.; Xiong, Q.; Sum, T. C. Tailoring the Lasing Modes in Semiconductor Nanowire Cavities Using Intrinsic Self-Absorption. *Nano Lett.* **2013**, *13*, 1080–1085.
29. Zhang, Q.; Li, G.; Liu, X.; Qian, F.; Li, Y.; Sum, T. C.; Lieber, C. M.; Xiong, Q. A Room-Temperature Low-Threshold Ultraviolet Plasmonic Nanolaser. *Nat. Commun.* **2014**, *5*, No. 4953.
30. Kondo, T.; Azuma, T.; Yuasa, T.; Ito, R. Biexciton Lasing in the Layered Perovskite-Type Material $(\text{C}_6\text{H}_{13}\text{NH}_3)_2\text{PbI}_4$. *Solid State Commun.* **1998**, *105*, 253–255.
31. Benoit La Guillaume, C.; Salvan, F.; Voos, M. Investigation of the Radiative Recombination of the Excitonic Molecule in Ge and Si. *J. Lumin.* **1970**, *1*–2, 315–323.
32. Renard, J.; Songmuang, R.; Bougerol, C.; Daudin, B.; Gayral, B. Exciton and Biexciton Luminescence from Single GaN/AlN Quantum Dots in Nanowires. *Nano Lett.* **2008**, *8*, 2092–2096.
33. Tanaka, K.; Hosoya, T.; Fukaya, R.; Takeda, J. A New Luminescence Due to an Exciton–Exciton Collision Process in Lead Iodide Induced by Two-Photon Absorption. *J. Lumin.* **2007**, *122*, 421–423.
34. Klimov, V. I.; Ivanov, S. A.; Nanda, J.; Achermann, M.; Bezel, I.; McGuire, J. A.; Piryatinski, A. Single-Exciton Optical Gain in Semiconductor Nanocrystals. *Nature* **2007**, *447*, 441–446.
35. Park, Y.-S.; Bae, W. K.; Pietryga, J. M.; Klimov, V. I. Auger Recombination of Biexcitons and Negative and Positive Triions in Individual Quantum Dots. *ACS Nano* **2014**, *8*, 7288–7296.
36. Fröhlich, D.; Kenkles, R. *Nuovo Cimento B* **1977**, *38*, 433–438.
37. Liu, X.; Zhang, Q.; Yip, J. N.; Xiong, Q.; Sum, T. C. Wavelength Tunable Single Nanowire Lasers Based on Surface Plasmon Polariton Enhanced Burstein–Moss Effect. *Nano Lett.* **2013**, *13*, 5336–5343.
38. Liu, X.; Zhang, Q.; Xing, G.; Xiong, Q.; Sum, T. C. Size-Dependent Exciton Recombination Dynamics in Single CdS Nanowires beyond the Quantum Confinement Regime. *J. Phys. Chem. C* **2013**, *117*, 10716–10722.
39. Citrin, D. S. Long Radiative Lifetimes of Biexcitons in $\text{GaAs}/\text{Al}_x\text{Ga}_{1-x}\text{As}$ Quantum Wells. *Phys. Rev. B* **1994**, *50*, 17655–17658.
40. Bacher, G.; Weigand, R.; Seufert, J.; Kulakovskii, V. D.; Gippius, N. A.; Forchel, A.; Leonardi, K.; Hommel, D. Biexciton versus Exciton Lifetime in a Single Semiconductor Quantum Dot. *Phys. Rev. Lett.* **1999**, *83*, 4417–4420.
41. Liu, X. F.; Wang, R.; Jiang, Y. P.; Zhang, Q.; Shan, X. Y.; Qiu, X. H. Thermal Conductivity Measurement of Individual CdS Nanowires Using Microphotoluminescence Spectroscopy. *J. Appl. Phys.* **2010**, *108*.
42. Varshni, Y. P. *Physica (Amsterdam)* **1967**, *34*, 149.
43. Honda, T.; Kawanishi, H.; Sakaguchi, T.; Koyama, F.; Iga, K. Characteristic Temperature Estimation for GaN-Based Lasers. *MRS Proc.* **1999**, *4*.
44. Ohtomo, A.; Tamura, K.; Kawasaki, M.; Makino, T.; Segawa, Y.; Tang, Z. K.; Wong, G. K. L.; Matsumoto, Y.; Koinuma, H. Room-Temperature Stimulated Emission of Excitons in $\text{ZnO}/(\text{Mg},\text{Zn})\text{O}$ Superlattices. *Appl. Phys. Lett.* **2000**, *77*, 2204–2206.
45. Wiersig, J. Hexagonal Dielectric Resonators and Microcavities Lasers. *Phys. Rev. A* **2003**, *67*.
46. Gargas, D. J.; Moore, M. C.; Ni, A.; Chang, S.-W.; Zhang, Z.; Chuang, S.-L.; Yang, P. Whispering Gallery Mode Lasing from Zinc Oxide Hexagonal Nanodisks. *ACS Nano* **2010**, *4*, 3270–3276.
47. Duan, X. F.; Huang, Y.; Agarwal, R.; Lieber, C. M. Single-Nanowire Electrically Driven Lasers. *Nature* **2003**, *421*, 241–245.
48. Tang, Z. K.; Wong, G. K. L.; Yu, P.; Kawasaki, M.; Ohtomo, A.; Koinuma, H.; Segawa, Y. Room-Temperature Ultraviolet Laser Emission from Self-Assembled ZnO Microcrystallite Thin Films. *Appl. Phys. Lett.* **1998**, *72*, 3270–3272.
49. Ushigome, R.; Fujita, M.; Sakai, A.; Baba, T.; Kubun, Y. K. GaInAsP Microdisk Injection Laser with Benzocyclobutene Polymer Cladding and Its Athermal Effect. *Jpn. J. Appl. Phys., Part 1* **2002**, *41*, 6364–6369.
50. Bhowmik, A. K. Polygonal Optical Cavities. *Appl. Opt.* **2000**, *39*, 3071–3075.
51. Liu, X.; Wu, B.; Zhang, Q.; Yip, J. N.; Yu, G.; Xiong, Q.; Mathews, N.; Sum, T. C. Elucidating the Localized Plasmonic Enhancement Effects from a Single Ag Nanowire in Organic Solar Cells. *ACS Nano* **2014**, *8*, 10101–10110.

Supporting information for

**Whispering Gallery Mode Lasing from Hexagonal Shaped
Layered Lead Iodide Crystals**

*Xinfeng Liu,^{1,2,#} Son Tung Ha,^{1,#} Qing Zhang,¹ Maria de la Mata,³ César Magen,⁴
Jordi Arbiol,^{3,5} Tze Chien Sum,^{1,2,6*} Qihua Xiong,^{1,2,7*}*

¹Division of Physics and Applied Physics, School of Physical and Mathematical Sciences, Nanyang Technological University, Singapore 637371

²Energy Research Institute @ NTU (ERI@N), Nanyang Technological University, 50 Nanyang Drive, Singapore 637553

³Institut de Ciencia de Materials de Barcelona, ICMAB-CSIC, E-08193 Bellaterra, CAT, Spain

⁴Laboratorio de Microscopías Avanzadas (LMA), Instituto de Nanociencia de Aragón (INA) - ARAID and Departamento de Física de la Materia Condensada, Universidad de Zaragoza, 50018 Zaragoza, Spain

⁵Institució Catalana de Recerca i Estudis Avançats (ICREA), 08010 Barcelona, CAT, Spain

⁶Singapore-Berkeley Research Initiative for Sustainable Energy, 1 Create Way, Singapore 138602

⁷NOVITAS, Nanoelectronics Centre of Excellence, School of Electrical and Electronic Engineering, Nanyang Technological University, Singapore, 639798

[#] These authors contribute equally to this work.

Ccorrespondences should be addressed, Email: Qihua@ntu.edu.sg and Tzechien@ntu.edu.sg

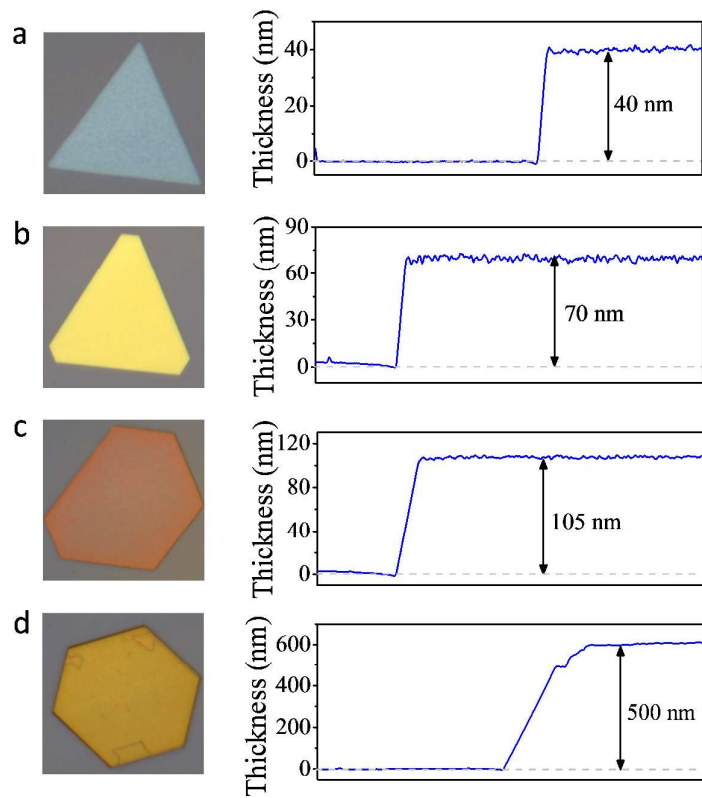


Figure S1 (a)-(d) Optical images and the corresponding thicknesses of four representative PbI_2 platelets. PbI_2 platelets show different colors for different thicknesses. From the AFM measurements, we know that the thicknesses of the four representative platelets are 40, 70, 105 and 500 nm respectively.

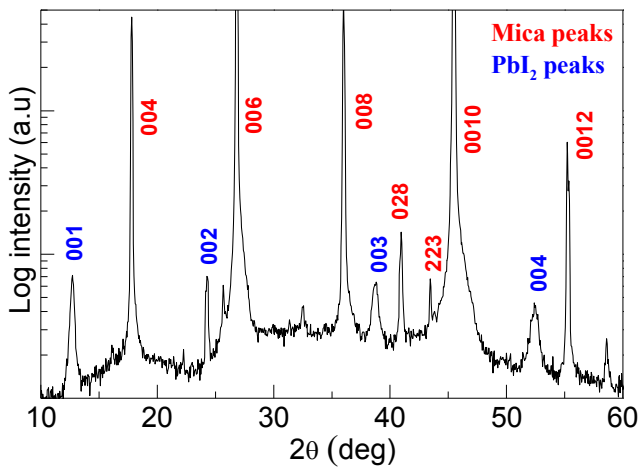


Figure S2 X-ray diffraction (XRD) pattern of the as-prepared sample on mica. The red and blue marked peaks are ascribed to mica and PbI_2 respectively.

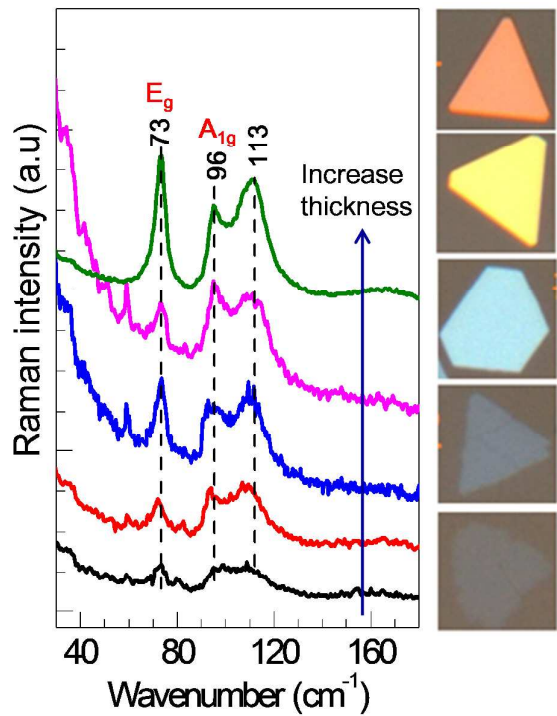


Figure S3 Raman spectra of the as-prepared platelets with different thicknesses, the excitation wavelength of 633 nm. The Raman peaks located at 96 and 73 cm^{-1} are attributed to the symmetric stretch A_{1g} and a doubly degenerate E_g band due to the shearing motion of two iodine layers. In addition, Raman band with peaks at 113 cm^{-1} are observed for the bulk 2H- PbI_2 . All these peaks are related to the structure of PbI_2 crystals.^[1]

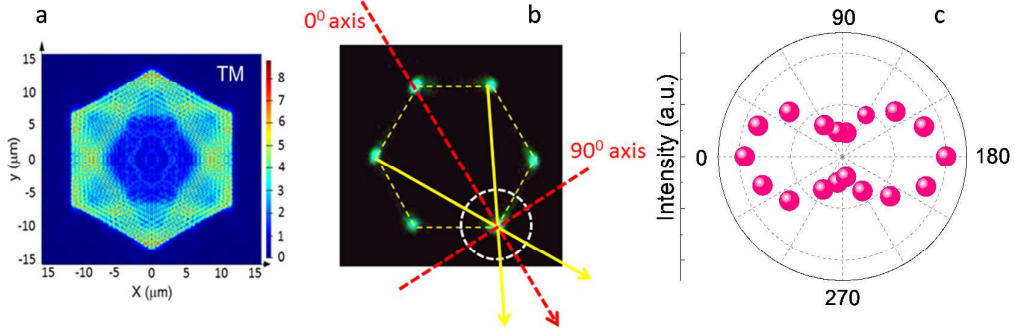


Figure S4 (a) The FDTD simulation of the electric distribution inside the cavity for hexagonal PbI₂ platelet (TM mode). (b) The scattering emission image of the PbI₂ platelet. The 0 and 90 degree axis are defined as shown in b. The white circle is the confocal area where we collected the scattering signal. (c) The measured polarization dependent lasing intensity. The relatively stronger signal along the 0 degree direction suggests that TM mode is dominant, which is consistent with our simulation result.

Figure S4a shows the simulation results of the electrical distribution inside the cavity (TM mode). To experimentally prove our simulation result, using confocal microscopy system, we measured the polarization dependent lasing intensities. The confocal area is confined using the white circle, as shown in Figure S4-b. The measured polarization dependent lasing intensity is exhibited in Figure S4-c. It can be seen that the lasing intensity shows a maximum when the polarization is along with the 0 degree axis, which suggests that the TM mode dominates the signal (if the TE mode dominates, the maximum signal happens when the polarization angle in 90 degree direction).

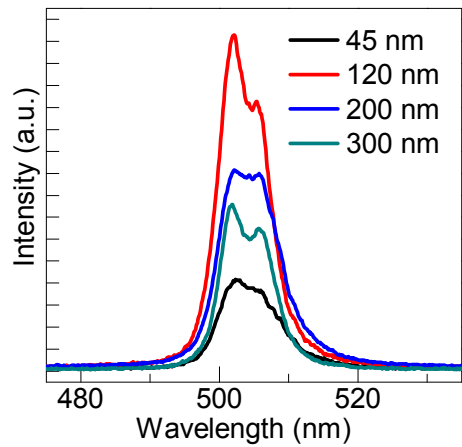


Figure S5 PL spectra of PbI₂ platelets with different thickness of 45, 120, 200 and 300 nm. These spectra are extracted from the streak camera images in the vertical direction. When the thickness is around 120 nm, a maximum PL intensity is observed.

References:

- [1] Gopi K Kasi, Norman R Dollahon and Temer S Ahmadi, Fabrication and Characterization of Solid PbI₂ Nanocrystals, *J. Phys. D: Appl. Phys.* **2007**, *40*, 1778–1783.